Solvent Effects on Cobalt Nanocrystal Synthesis-A Facile Strategy To Control the Size of Co Nanocrystals

Salvatore Costanzo, Guilhem Simon, Johannes Richardi, Philippe Colomban, Isabelle Lisiecki

DOI: 10.1021/acs.jpcc.6b07293

Solvent Effects on Cobalt Nanocrystal Synthesis - A Facile Strategy to Control the Size of Co Nanocrystals

S. Costanzo[a,b], G. Simon[a,b], J. Richardi[a,b], Ph. Colomban[a,b], I. Lisiecki [a,b,*]

a Sorbonne Universités, UPMC Univ Paris 06, UMR 8233, MONARIS, 4 Place Jussieu, 75005, Paris, France

b CNRS, UMR 8233, MONARIS, 4 Place Jussieu, 75005, Paris, France

Corresponding author :

Mail : Isabelle.lisiecki@upmc.fr

Tel : 0033-144272021

ABSTRACT

In this paper, revisiting the chemical reduction approach of $Co(AOT)_2$ (AOT = bis(2-ethylhexyl)sulfosuccinate) precursor by $NaBH_4$, we highlight a novel synthetic strategy based on the change of the solvent to accurately control the size of Co nanocrystals (NCs) from 3.9 to 9.3 nm and their 2D and 3D (supracrystal) ordering. The evolution of the NC size with the solvent is explained by solvent mediated ligand-ligand interactions using Hansen solubility parameters. A formula for the nanocrystal size as a function of the solvent is proposed which predicts its diameter within 1 nm. Moreover, and to the best of our knowledge, we show the first example of tunable Co NC size while keeping unchanged the chemistry of ligands (combination and proportion) during the growth step. Due to the possibility we have to replace the AOT ligand by the strong-binding dodecanoic acid, Co NCs are characterized by long-term stability against oxidation and coalescence of the metallic NCs, whatever their size is. Low wavenumber Raman spectra are obtained using a triple notch filtered spectrometer under the 514.5 nm excitation. Two modes are clearly observed according to Lamb's model of sphere vibrations whatever the excitation laser line is far away from Plasmon absorption. They shift linearly with inverse particle diameter from ~ 8/17 ±0.1 cm^{-1} (9.3 nm) to 12.5/23 ± 0.3 cm^{-1} (3.9 nm).

1 INTRODUCTION

Magnetic nanocrystals (NCs) have gained increased interest in the past two decades due to their potential applications in ultrahigh density information storage, electronics, sensors and drug delivery systems.[1,2] The physico-chemical properties of these NCs, strongly depend on their size,[3-7] shape,[8-10] crystallinity[11-15] and surface chemistry,[16] which then have to be finely controlled. In order to probe the fundamental size-dependent properties of metallic NCs, it is crucial to synthesize size-tunable monodispersed NCs while keeping other structural parameters unchanged. Due to their uniform size, such NCs may then be used as building blocks for ordered assemblies (superlattices). In the case of Co, size-controlled colloidal synthesis of spherical metallic NCs remains, to this day, a challenge, and few strategies exist for this to address this challenge.[4,5] Such strategies are based either on decomposition of organometallic precursors or metal salt reduction. In thermal decomposition of organometallic precursor, a suitable precursor (e.g $Co_2(CO)_8$) is rapidly decomposed at high temperatures in presence of surfactants and the NC size is tuned by tailoring the reaction time, reaction temperature, precursor injection time, surfactant to precursor ratio and chemistry of reagents and surfactants. The first such example of size-controlled of monodisperse and spherical Co NCs using this approach has been reported by Alivisatos and co-workers.[5] Another approach for formation of size-controlled Co NCs is the metal-salt chemical reduction first reported by Murray and Sun.[4] In this method typically, a reducing agent is injected into a hot solution of metal precursor ($CoCl_2$ or $Co(CH_3COO)_2$) in the presence of surfactants. For both approaches, it should be noted that surfactant is the key parameter not only in the stability of the NCs against coalescence and oxidation but also in mediating the NC growth. In most cases, a combination of two or three surfactants is employed, where in one binds tightly to the metal NC surface (e.g. oleic acid) favouring slow growth, while and the other(s) bind weakly allowing a rapid growth (e.g., alkylphosphine,[4,12] phosphonic acid,[6] alkylamine.[17]). NC size is tuned by selecting the nature of surfactants and their concentration ratio. In view of this, the surface chemistry of Co NCs varies from a size to the other one while the physico-chemical properties can significantly depend on it. Furthermore, the choice of the surfactants, which is dictated by the desired NC size, always includes a weak-binding molecule, which may explain the lack of stabilization of the Co NCs. This point is important because

this may make impossible annealing treatments that could be required to control the material crystallinity.

In this paper, we report a new and simple synthetic strategy based on the solvent-mediated AOT ligand (AOT = bis(2-ethylhexyl)sulfosuccinate) interactions for an accurate and reproducible step control over the size (from 3.9 to 9.3 nm) of uniform Co NCs. To this end, we revisit the chemical reduction approach of $Co(AOT)_2$ precursor by $NaBH_4$ at room temperature.[7] Conversely to the previous reported results, Co NC growth is not controlled by selecting the suitable combination of surfactants and their concentration ratio but just by selecting the suitable solvent. Indeed, we show that the AOT surfactant solvation is the key parameter that determines the strength and range of AOT-AOT interactions, which drive the growth of the metallic NCs. Finally, the use of the strong binding dodecanoic acid coating agent to replace the AOT surfactant after the growth step provides an efficient stabilization of the NCs.[18] At the end of the full process, we obtain size tunable Co NCs, stabilizing with identical and single coating agent, and characterized by a higher stability compared to the reported Co NCs partly stabilized by coating agents comprised weak one's. Such highly stable NCs, are used as building blocks in 2D and 3D superlattices. Interestingly, this novel strategy based on the solvent-mediated ligand interactions to control the growth of Co NC size would provide a useful guide in the choice of solvent for size-controlled synthesis of inorganic NCs, whatever the material is. A comprehensive characterisation of Co NCs and the 2D and 3D is performed using Transmission Electron Microscopy and low-wavenumber Raman scattering.

2 EXPERIMENTAL SECTION

2.1 Products. All materials were used without further purification. Cobalt acetate and dodecanoic acid are from Aldrich; isooctane, hexane, cyclohexane, xylene, cumene, decane, octane are from Sigma Aldrich, and sodium di(ethylhexyl) sulfosuccinate (Na(AOT)) is from Fluka; sodium borohydride and dodecanoic acid are from Acros. The synthesis of cobalt(II) bis(2-ethylhexyl)sulfosuccinate, ($Co(AOT)_2$) has been described previously.[19]

2.2 Apparatus. Transmission electron microscopy (TEM) was performed using a JEOL JEM-1011 microscope at 100 kV. High-resolution transmission electron microscopy (HRTEM) was performed using a JEOL 2010 microscope at 200 kV and

using a Nion Ultrastem 100 scanning transmission electron microscope operating at 100 kV. The Nion Ultrastem 100 microscope is equipped with a spherical aberration corrector, which enables a probe size of under 0.1 nm to be obtained, although the spatial resolution here was slightly worse due to an alignment problem. The FT optical images are visualized with the Digital Micrograph software by Gatan.
A HR800 LabRam setup from Horiba Scientific Jobin Yvon, working with 514.5-nm laser excitation and equipped with BragGrate notch filters from Optigrate were used for all Raman measurements. We used a ×100 microscope objective (Olympus, NA: 0.90), for which the spot diameter at the focal point was small enough (~1 μm) to fully illuminate a definite surface area of the assembly. The resolution of spectrometer in the experimental condition was about of 1 cm^{-1}. In order to compare the scattering efficiencies, the laser power was locked around 100 μW (at the focal point), and care was taken to always focus the same way on different samples. Apart from a constant background subtraction by a straight line when required, all the spectra are raw data. Note that low illumination power does not guarantee any absence of heating. Raman Intensities are normalized taking into account the intensity of the stronger band in order to evidence the band shift due to the particles size. The data are the average of three experiments done in the same condition, the error bars in the linear regression are made up from the linear fitting.

2.3 Size histograms. The histograms of the NCs are obtained by measuring the diameter D_i of at least 500 NCs deposited on a grid coated with amorphous carbon. The relative standard deviation, σ_r, is calculated from the experimentally determined distribution using the formula:

$$\sigma_r = \frac{100\ x \sqrt{\sum_{i=1}^{500} \frac{\left(D_i - D_{avg}\right)^2}{n-1}}}{D_{avg}} \qquad (1)$$

Where *n* corresponds to the number of measured particles, D_{avg} is the average diameter of the population and D_i is the i^{th} particle diameter expressed in nm.
The average inter-particle spacing is measured by taking into account alignments of about fifty particles in three different orientations in the 2D ordered assemblies.

2.4 Synthesis of metallic cobalt NPs. Co NPs are synthesized by room temperature solution phase reduction method. Six different solutions of $5x10^{-2}$ M $Co(AOT)_2$ are prepared using xylene (S*1*), cyclohexane (S*2*), cumene (S*3*), decane

(S*4*), octane (S*5*), and isooctane (S*6*) as bulk solvent. The amount of water added in solution is fixed to reach a water concentration defined as $w=[H_2O]/[AOT]$ is *2*. These prepared microemulsions are vigorously shacked for few minutes for equilibrium and form reverse micelles.[20-23] An aqueous solution of 1 M $NaBH_4$ is added to these systems, so that the reducing agent content, *R* ($R=[NaBH_4]/[Co(AOT)_2]$) is *6.*[7] As a consequence of the high volume of aqueous solution brought by the reducing agent introduced, reverse micelles are instantaneously destroyed.[22-23] Under vigorous shacking, the solution instantaneously turns from purple to black indicating the reduction of Co^{2+} ions followed by the nucleation and growth of Co NCs. After synthesis, the Co NCs are extracted from the AOT surfactant by adding dodecanoic acid molecules. After washing several times with ethanol the NCs are dispersed in hexane. The six resulting colloidal solutions *S1*, *S2, S3*, *S4, S5* and *S6* synthesized respectively with xylene, cyclohexane, cumene, decane, octane and isooctane as bulk solvent, are then centrifuged to precipitate bulky materials and we collect the upper phase containing dispersed NCs in hexane. A seventh colloidal solution of Co NCs, *S7,* is obtained after removing the upper phase of sample S6 and by dispersing a part of the precipitate containing Co NCs, in cyclohexane. The syntheses are carried out at room temperature, in a nitrogen glove box using de-oxygenated solvents to prevent particle oxidation.

2.5 Assembly preparation. 2D ordered assemblies are prepared by depositing 1 drop of a colloidal solution, in which the concentration of Co NCs is fixed at 5.5×10^{-7} M, on highly ordered pyrolytic graphite (HOPG) grid placed on a sheet of paper. To prepare the HOPG grids, a sheet of HOPG is stuck on an untreated copper grid. The HOPG is then cleaved to give a very thin layer, permitting TEM observations**.** Thin 3D ordered assembly are prepared by depositing 1 drop of a colloidal solution, in which the concentration of Co NCs is fixed at 5.5×10^{-7} M, on HOPG TEM grid placed on graphite support. To prepare the 3D thick superlattices for Raman study, HOPG substrates (10 mm x 5 mm) are horizontally immersed in 200 µL of 5.5×10^{-7} M colloidal NC solution. The solvent evaporation takes place at 35°C under nitrogen flow.

2.6 Calculation of interaction parameters. To understand the dependence of the NC diameter on the solvent, the solubility parameter as proposed by Hansen is used.[24,25] The interaction parameter χ_{12} is calculated from the usual equations:

$$\chi_{12} = V_s A_{1,2} / R T \text{ with } A_{1,2} = (\delta_{D2}-\delta_{D1})^2+0.25(\delta_{P2}-\delta_{P1})^2+0.25\ (\delta_{H2}-\delta_{H1})^2 \quad (2)$$

δ_D, δ_P and δ_H are the Hansen solubility parameters for the dispersion, polar and hydrogen bonding interactions, respectively (**Table 1**). Index 1 and 2 denote the solvent and the ligand. V_s is the molar volume of the solvent. R and T are the ideal gas constant and the temperature (here 298.15 K). The solubility parameters and molar volumes are mainly taken from CRC Handbooks.[25]

In a computer simulation of the formation of cobalt NCs in toluene,[26] it was shown that the polar group of the AOT binds to the NC surface while the aliphatic tail is in contact with the solvent. Therefore, the solubility parameters of the alkyl chain of the tails have to be used to calculate χ_{12}. Following refs,[27-28] we use the longest alkyl chain to fix the solubility parameters. Therefore, the values for hexane and dodecane are used for the Hansen solubility parameters of AOT and dodecanoic acid. Please note that the ligand may desorb from the nano crystal surface during the growth process, but it can be assumed that these ligand molecules do not play an important role for the further NC growth.

Table 1. Solvent volume, (V_s), Hansen solubility parameters[24] related to London dispersion force (δ_D), polar interactions (δ_P) and hydrogen bond (δ_H)

Solvent	V_s (cm^3mol^{-1})	δ_D ($MPa^{1/2}$)	δ_P ($MPa^{1/2}$)	δ_H ($MPa^{1/2}$)
Hexane	131.6	14.9	0.0	0.0
Octane	163.5	15.5	0.0	0.0
Isooctane	166.1	14.3	0.0	0.0
Decane	195.9	15.7	0.0	0.0
Dodecane	228.6	16.0	0.0	0.0
Cyclohexane	108.7	16.8	0.0	0.2
Xylene	123.3	17.6	1.0	3.1
Cumene	123.1	17.8	0.6	1.4

3 RESULTS AND DISCUSSION

3.1 Synthesis and structural characterization of size-tunable monodisperse dodecanoic acid-coated Co NCs. From the TEM investigation of the colloidal solution, we infer that the mean diameter of the Co NCs synthesized by reduction of $Co(AOT)_2$ precursors with $NaBH_4$, significantly depends on the combination of the AOT solvent and the solvent used to solubilize the dodecanoic acid coated Co NCs, named C_{12}-NC solvent. Using hexane as the C_{12}-NC solvent, the mean diameters of the Co NCs are found to be 3.9, 4.6, 4.7, 7.0, 7.6 and 7.7 nm

for xylene, cyclohexane, cumene, decane, octane and isooctane used as AOT solvents respectively, while the corresponding size distributions remain narrow, (σ ~ 12%, **Table 2**). TEM images (**Figure 1a-d**) and corresponding size histograms (**Figure 2(a)**) illustrate this behaviour for S1, S2 and S6 samples. Using UV-vis spectroscopy, the volume fractions of cobalt defined as the ratio of cobalt in colloidal solution to the one initially used for the synthesis, have been estimated. They are found almost the same (around 11%) for all the samples. Moreover, a careful investigation of the precipitate coexisting with the colloidal solution is performed by TEM. It shows that it is mainly made of coalesced particles with a minor fraction of aggregated particles. This fraction of particles can be re-dispersed by using another solvent as explained in the following section.

Table 2. Sample Sx; AOT solvent/C12 NC solvent; Diameter and σ_r.

Sample	***AOT-Solvent /NCs-Solvent***	D_{avg} ***(nm)***	σ_r ***(%)***
S1	Xylene / hexane	3.9	12
S2	Cyclohexane /hexane	4.6	11
S3	Cumene/hexane	4.7	11
S4	Decane/hexane	7.0	12
S5	Octane/hexane	7.6	11
S6	Isooctane/hexane	7.7	12
S7	Isooctane/cyclohexane	9.3	15

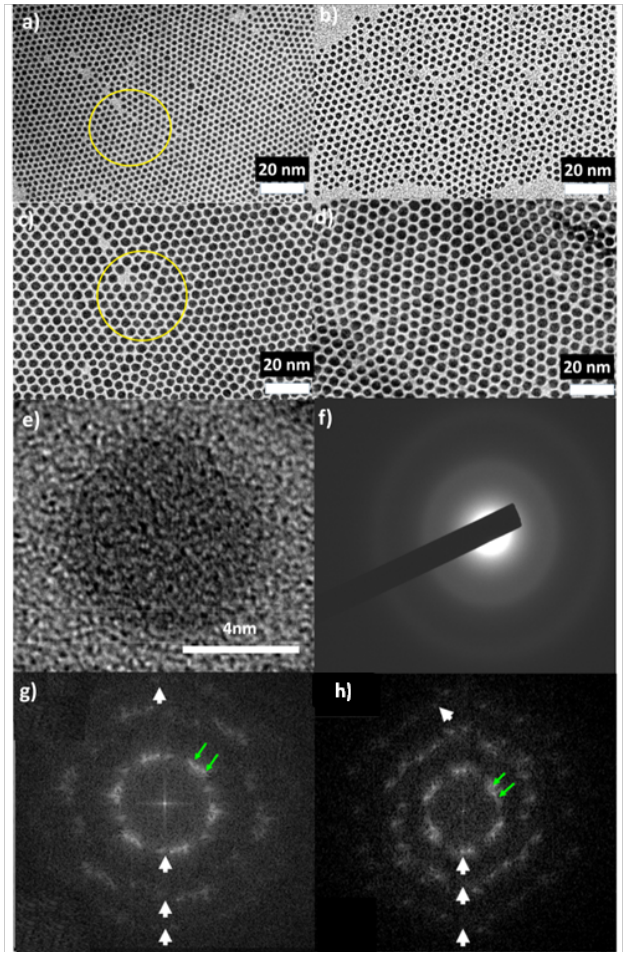

Figure 1. TEM micrograph of 2D ordered assemblies of Co NCs (a) 3.9 nm (S1), (b) 4.6 nm (S2), (c) 7.7 nm (S6) and (d) 9.3 nm (S7). (e) High-Resolution TEM micrograph of a single NC of (S3). (f) Electron diffraction pattern of 2D assembly of Co NCs of 7.7nm. (g) and (h) Optical Fourier Transform of selected area of Fig a and c.

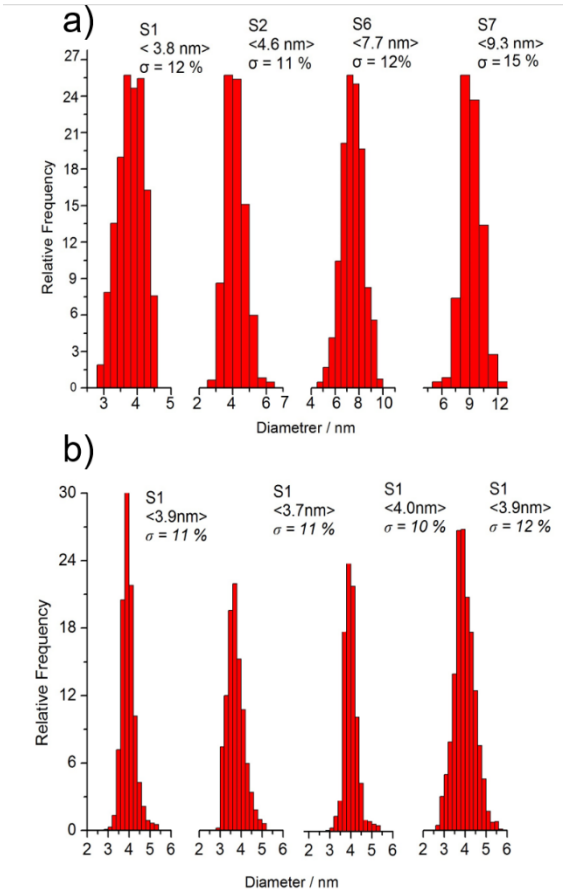

Figure 2. (a) Size distribution of Co NCs shown in the Fig. 1 (a-d) made at different bulk organic solvents. (b) Size distribution of Co NCs (sample S1) made up from several syntheses.

A seventh colloidal solution of Co NCs, *S7,* is obtained after removing the upper phase of sample S6 (performed with isooctane as AOT solvent and hexane as C_{12}-NC solvent) and by dispersing a part of the precipitate containing Co NCs, in cyclohexane. TEM study (**Figure 1d** and **2a**) shows that this "second dispersion" (in cyclohexane) is composed of NCs with a mean diameter of 9.3 nm against 7.7 nm for the "first dispersion" (in hexane) (S6, (**Figure 1c** and **2a**)). **Obviously, cyclohexane allows the extraction of the upper tail of the size distribution, which is not soluble in hexane**. The size distribution slightly increases from 12 to 15%. The volume fraction of S7, estimated by UV-vis spectroscopy, is found equal to 4 %. This shows that the fraction of larger particle dispersed by cyclohexane is considerably low.

In order to check the reproducibility of the experiments, we included in **Figure 2b** the size histograms of Co NCs from four syntheses performed under the same conditions as S1 for comparison. The variations of the mean diameter observed from

sample to sample are very low and (almost near to the error of the size determination by TEM about 0.1 nm) the size distribution always remains below 12% (**Figure. 2b**). Despite these very small variations in the mean diameter, the general trend of an accurate control of the size of Co NCs with our synthetic approach is clear. Regardless of the population is, it appears that Co NCs are not perfectly spherical. That is all the more visible with the biggest NCs, which appear more or less ovoid (**Figure 1b**) or pentagonal (**Figure 1d**). HRTEM study shows that few small crystalline domains with a typical size smaller than 1 nm constitute these NCs (**Figure 1e**). The highly disordered polycrystalline structure of Co nanoparticles is further confirmed by the electron diffraction pattern displaying two diffuse rings at 0.204 ± 0.001 nm and 0.120 ± 0.001 nm, which could be indexed as the (111) and (220) reflections respectively of fcc-Co (**Figure 1f**). Regardless the particle environment (e.g., isolated or organized in superlattices), no presence of oxide is detected.

3.2 Why AOT reverse micelles do not play the role of nanoreactors? It is now well established that chemical reduction within the aqueous cores of water-in-oil AOT reverse micelles is an effective method for the production of size-controlled NCs while maintaining a narrow size distribution.[29-33] The key parameters involved in this synthetic strategy are both the size of the water droplet [34,35] and the rate of micellar exchange.[7,36-38] However, it is important to highlight that, in the present work $Co(AOT)_2$ reverse micelles do not play the role of nanoreactors. As mentioned above, the reduction step is performed by the injection of an aqueous $NaBH_4$ solution, the volume of which is too high to ensure the integrity of the water droplets. Consequently, in our case, the mechanisms governing Co NC formation are not those involving in reverse micelles. This behavioural divergence is well-illustrated by various observations. It is noted that for all other conditions equal, the size of Co NCs remains constant with the variation of water content, *w*, of the initial reverse micelles. For instance, using isooctane as the AOT solvent, we report here that the mean diameter of Co NCs is found to be equal to 7.7 nm at w=2 compared to 7.5 nm at w=32.[13] At w=2 and w=32, the mean diameter of the micelles are respectively equal to 1.0 nm and 6.0 nm.[22,23] On the other hand, at a fixed w value, (w=32), synthesis performed at various concentrations of $Co(AOT)_2$ always give rise to the same mean diameter of Co NCs, i.e. around 7.5 nm.[39] For these two series of experiments, if the

NC formation would really occur in the micellar system, Co NCs size would be expected to significantly change with w value and with the intermicellar exchange process driven by the concentration of $Co(AOT)_2$, i.e. the polar volume fraction.[35] These results further illustrate the absence of reverse micelles during the Co NCs formation.

3.3 Key role of the solvent in the size control of Co NCs. Actually, synthesis of Co NCs is occurring in a ternary component system (Co(AOT)2, oil, water) whose phase diagram is strongly perturbed by the injection of a high volume of reducing agent. Such a complex system makes it difficult to identify the key parameters involved in size control. Nevertheless, we propose the following interpretation of our results. Control of the Co NC size is mainly explained in terms of competition between the interactions solvent/AOT, AOT/AOT and AOT/metal Co. Changing the nature of the solvent significantly impacts the AOT solvation and then the final size of Co NC. Indeed, the growth of Co NCs is driven by the AOT adsorption on the metal surface induced by the attraction between the cobalt atoms and the polar head groups of AOT but also by AOT/AOT interactions.[40] Tuning the AOT solvation provides an efficient way to control the AOT/AOT interactions and then the final metal NC size. In order to support our statement, the χ_{12} parameters were calculated and are compared to the experimental NC diameters in **Table 3**.

Table 3. Calculated χ_{12} parameters and experimental NC diameters for solvent-ligand pairs used in the experiments.

Solvent – ligand	***χ_{12} (J mol^{-1})***	***NC diameter (nm)***
Octane – AOT	0.02375	7.6
Isooctane – AOT	0.02412	7.7
Decane – AOT	0.05058	7.0
Cyclohexane – AOT	0.17272	4.6
Cumene – AOT	0.44645	4.7
Xylene – AOT	0.49455	3.9
Hexane – C12	0.06424	7.7
Cyclohexane – C12	0.03062	9.3

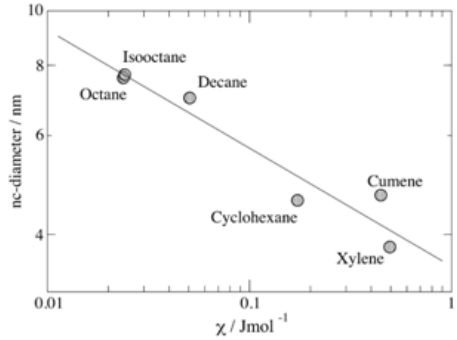

Figure 3. Log-log plot of the experimental NC size and the interaction parameter.

The NC size decreases as the χ_{12} parameter increases. In **Figure 3**, the NC diameter is plotted against the χ_{12} parameter using logarithmic scale. A linear regression gives:

$$\log (d) = 0.944 - 0.211 \log (\chi_{12}) \quad (3)$$

d and χ_{12} being expressed in nm and $Jmol^{-1}$, respectively. Based on our results, this formula yields the NC diameter within an error of ~1 nm.

This result may be interpreted as follows. A larger χ_{12} value usually favours the attraction between the ligands due to the surrounding solvent. But how does this stronger ligand-ligand attraction influence the NC growth? The NC growth can be separated into two steps. In the first step, small Co crystals nucleate, while in the second step these crystals continuously grow. The first nucleation step is mainly determined by the Co-Co interactions. DFT calculations,[26] show that the Co-Co interactions are significantly stronger than the interactions between the solvent and the cobalt atoms. Therefore, we assume that the nucleation is not largely modified by the solvent. However, in the second step, a ligand layer is formed on the NC surface, which slows down the crystal growth. The formation and solidity of the ligand layer is mainly determined by Co-ligand interactions but also influenced by ligand-ligand interactions. As explained above, the ligand-ligand attraction increases due to larger χ_{12} parameters such as for cyclohexane, xylene and cumene. This increases the stability of the ligand layer and thus hinders the growth process of the nanocrystal for theses solvents. This explains why an increase in the χ_{12} value leads to smaller nanocrystal as observed in experiments.

The χ_{12} interaction parameters may also explain the larger NC size obtained by an extraction with cyclohexane (S7) compared to hexane (S6). While the former

discussion focuses on the interactions for a single NC, we study here the attraction between two NCs. It must also be noticed that here the ligand has changed and we have to use dodecane as ligand tail instead of hexane for AOT. The χ_{12} parameters were calculated for dodecane as ligand using cyclohexane (**0.0306 J mol^{-1}**) and hexane (**0.0642 J mol^{-1}**) as solvents. The lower χ_{12} value shows that cyclohexane is a better solvent, since it corresponds to lower ligand induced attractions between the nanocrystals and, thus, a decrease in particle aggregation. It is important to note that the ligand induced attraction between the nanoparticles usually increases with the nanocrystal size. This explains that lower χ_{12} values corresponding to a weaker ligand-ligand attraction may allow the extraction of NCs with larger diameters in good agreement with the experiment.

It is highly interesting to note that similar solvent-mediated ligand interactions have been recently reported to explain the growth of supracrystals of Au NCs.[28] The authors evidenced from experiments and simulations, that the degree of affinity of the solvent for the coating agent of Au NCs, i.e., its solvation, is one of the key parameter in the final morphology of periodic arrangements with either a layer-by-layer growth or a process of nucleation and growth in solution. Such finding strengthens our explanation for Co NC growth but not only. The similarity in the nucleation and growth mechanisms of both NCs and supracrystals of NCs allows us to do an analogy related to the physical behaviours at both atomic and NC scales.[28,41-43] This novel strategy using the solvent-mediated ligand interaction allows accurately controlling the growth of Co NC size but not only as all the NCs with tunable sizes are stabilized with the same coating agent. As the physico-chemical properties including the oxidation process and the magnetism related to the pinning of the surface spins, are strongly dependent on the surface chemistry of NCs, keeping constant their coating agent is highly required. Moreover, this strategy would provide a useful guide in the choice of solvent for size-controlled synthesis of NCs, whatever the material is.

Table 4. Average diameter of Co NCs (D_{avg}), size distribution (σ_r), centre-to-centre distance ($D_{c\text{-}c}$), inter-particle spacing ($D_{i\text{-}p}$).

Colloidal solution	*AOT solvent/ C12-NC solvent*	D_{avg} *(nm)*	σ_r *(%)*	D_{c-c} *(nm)*	D_{i-p} *(nm)*
S1	Xylene/hexane	3.9 ± 0.1	12	5.9 ±0.1	2.1±0.1
S3	Cyclohexane/hexane	4.6 ± 0.1	11	6.9 ±0.1	2.3±0.1
S6	Isooctane/hexane	7.7 ± 0.1	12	9.3 ±0.1	1.6±0.1
S7	Isooctane/cyclohexane	9.3 ± 0.1	15	10.5±0.1	1.4±0.1

3.4 2D and 3D ordered assemblies of Co NCs (**Table 4** and **Figure 4**)**.** As a result of the balance between surface tension, Van der Waals forces and magnetic interactions between superparamagnetic NCs, Co NCs, whatever their size is, self-organise into 2D and 3D long-range assemblies. **A low size dispersion of the NPs coupled to the size segregation favours such long-range self-organisation of metallic NPs**. TEM micrographs (**Figure 1a-d**) illustrate here this behaviour for samples S1, S3, S6 and S7, and show that the drop-wise deposition of colloidal NC solutions on a TEM grid (supported on a paper sheet) composed of a thin layer of highly ordered pyrolytic graphite (HOPG) gives rise to 2D self-organization of Co NCs with hexagonal symmetry. These 2D assemblies are determined by the size of the NC and the thickness of the coating agent. For 3.9 nm Co NCs, (**Figure 1a, Table 4**), the 2D array is characterized by a mean centre-to-centre distance between particles (D_{c-c}) of 5.9 nm and an inter-particle spacing (D_{i-p}) of 2.1 nm. The length of dodecanoic acid molecule being 1.77 nm, D_{i-p} thus indicates a dense lateral packing likely resulting from the inter-digitation of the C_{12} alkyl chains. Higher NC diameters lead to a significant decrease in the D_{i-p}. For Co NCs characterized by a mean diameter of 4.6, 7.7 and 9.3 nm, the D_{i-p} values are respectively equal to 2.3, 1.6 and 1.4 nm (**Table 4**). Such a variation of the NC packing is mostly explained in terms of Van der Waals attractions between the metallic NCs, which increase with their volume. The 2D hexagonal packing of ordered Co NCs is further evidenced by the optical Fourier-transform made on the selected area of TEM micrographs [shown in white circles in **Figure 1a** and **1c**], which reveals a hexagonal diffraction pattern (**Figure 1g** and **1h**). In the same figures, the long-range 2D organisation of NCs is evidenced by the 3 orders of diffraction (bold arrows). The splitting of the spots (light arrows) resulting from twinning is also visible.

Thin 3D ordered assemblies are obtained by drop-wise deposition of the colloidal solution on a HOPG TEM grid placed on a graphite substrate. This deposition

method is intermediate between the drop-wise deposition on HOPG TEM grid supported on a paper sheet for 2D assembly, and the dipping method employed to produce samples for Raman spectroscopy. In this deposition protocol, the colloidal solution does not evaporate rapidly since the HOPG substrate hinders the fast evaporation and Co NCs form thin multi-layered ordered assemblies. Regardless of the Co NC size, they self-organise in thin 3D superlattices composed of few monolayers of NCs (less than 5) with regular lattice planes. Shown in **Figure 4a** and **4b** are TEM micrographs of 3D assemblies of 3.9 nm (S1) and 7.7 nm (S6) Co NCs. The corresponding optical Fourier transforms made on the selected areas of TEM micrographs (**Figure 4c** and **4d**) yields a 6-fold symmetry pattern made of rather narrow spots showing the high level of organization of the NCs in these assemblies. For Raman spectroscopy, thicker 3D assemblies are produced by immersing HOPG substrates in the colloidal solutions (S1-S4) under nitrogen flow at 35°C. Such assemblies are composed of several tens of layers of NCs and their mesostructures depend on the NC size. The smallest NCs (D_{avg}=3.9 nm) assemble to form flower-like mesostructures (**Figure 4e**). Larger NCs give rise to a more uniform film (**Figure 4f**) in good agreement with a previous study.[44]

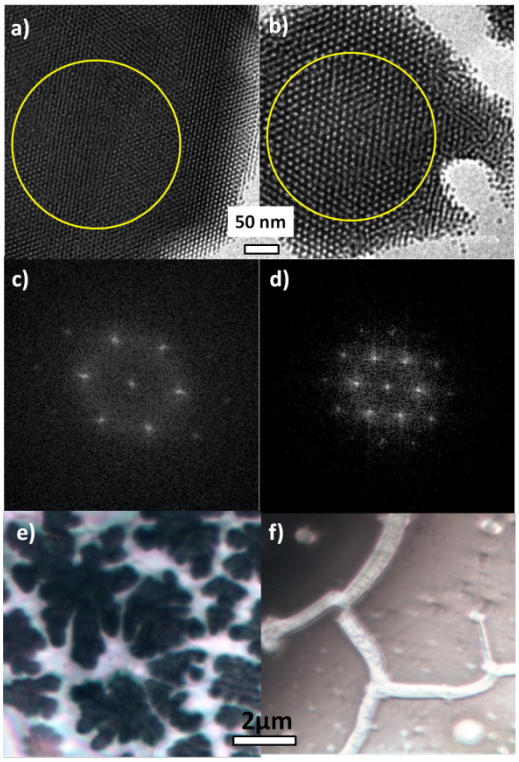

Figure 4. TEM micrographs of thin 3D ordered assembly of Co NCs of (a) 3.9 nm (S1) and (b) 7.7nm (S6). Optical Fourier Transforms made on the circles from (a) (c)

and from (b) (d). Optical images of thicker 3D assemblies of Co NCs (e) 3.9nm and (f) 7.7nm.

3.5 Low-wavenumber Raman scattering. Figure 5a compares the representative anti-Stokes – Stokes Raman spectrum characteristic for each synthesis (D_{avg}=3.9, 4.6, 7.7 and 9.3 nm). According to Lamb's theory,[45-47] the vibration modes of a free elastic sphere (regular) are described with the azimuthal quantum number ℓ. From the selection rules established in references,[46-48] Raman-active modes are characterized by an even quantum value of ℓ. The lowest wavenumber has a peak at ~10 cm^{-1}, is assigned to the quadrupolar (ℓ=2) mode; and the peak at ~20 cm^{-1} to the breathing mode (ℓ=0).[49] The narrow size distribution and high stability of NCs against oxidation and coalescence, combined with the high luminosity of the spectrometer at the particular wavenumber interval made possible the simultaneous observation of both breathing and quadrupolar modes whatever the Plasmon absorption of cobalt metal is expected far away from the laser excitation energy[49]. Variation of the quadrupolar and breathing mode wavenumber as a function of the inverse particle diameter shows a linear behavior as expected (**Figure 5b**).[45,47] The wavenumber of the breathing mode is also in accordance with previous results obtained through femtosecond pump-probe spectroscopy[14] on Co samples prepared with the same route, as well as with previous characterization of 3D assemblies of 7.7 nm Co NCs.[49] Note a supplementary spectrum exhibiting broader Raman signature can be observed in some spot for Co NCs having D_{avg}=4.6 nm in accordance with the non-spheroidal shape of our nanoparticles. However, loss of spherical symmetry leads to more active modes[50] that causes a broadening of peaks.

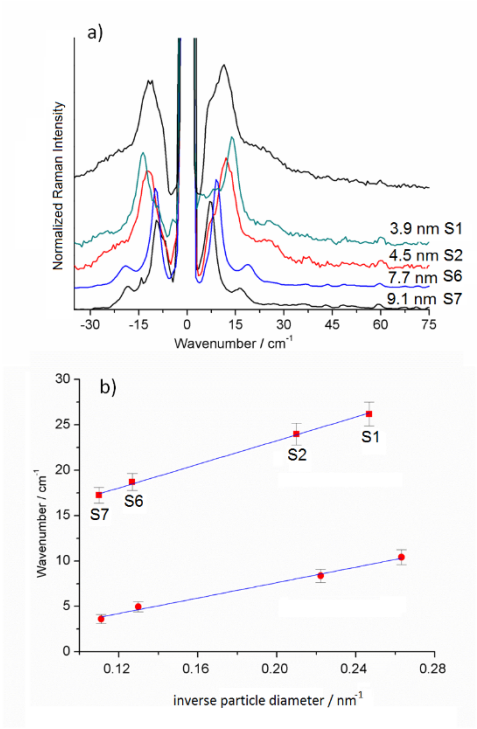

Figure 5. Representative low Wavenumber Raman Spectra of Co NCs with different diameter. The spectra are vertically shifted for clarity. The upper spectrum is related to ovoid particles (a). Plot of mean wavenumber of quadrupolar (circles) and breathing **(squares) modes as a function of the inverse particle diameter (b).**

4 CONCLUSION

Revisiting the chemical reduction approach of $Co(AOT)_2$ precursors with $NaBH_4$ as reducing agent, we highlight a novel synthetic strategy based on solvent-mediated ligand (AOT and dodecanoic acid) interactions to accurately control the size of Co nanocrystals (NCs) from 3.9 to 9.3 nm and their 2D and 3D ordering. The evolution of the NC size is explained by solvent-mediated interactions, which allows predicting the NC diameter within a precision of ~1 nm using equation (3). This synthetic strategy, allows not only to tune, in a reproducible way, the metallic NC size but also to keep the same coating agent for all the sizes, here, the strong binding dodecanoic acid one's that is all the more required to probe the size effect on the physico-chemical properties. Due to the high stability against oxidation of the different Co NCs, they spontaneously form long-range 2D and 3D ordered assemblies. According the Lamb's model of sphere vibrations, low wavenumber Raman study shows two vibration modes, clearly observed whatever the exciting laser wavelength don't interact with the cobalt Plasmon absorption. Low wavenumber Raman spectroscopy appears a good technique to determine the metal particle size. An easy and reliable

size and shape control of NCs will play an important role in the future development of nanotechnology. Therefore, the role of solvent revealed in our study may have an important impact for many nanoscale systems.[51-55]

ACKNOWLEDGMENTS

The research leading to these results has been supported by a grant ANR-CE08-007 from the ANR French Agency. We are grateful to Mathilde Chaboud for her technical support for Raman spectrometer.

REFERENCES

(1) Lu, A. H.; Salabas, E. L.; Schüth, F. Magnetic Nanoparticles: Synthesis, Protection, Functionalization, and Application. *Angew. Chem. Int. Ed. Engl.* **2007**, *46*, 1222–1244.

(2) Singamaneni, S.; Bliznyuk, V. N.; Binek, C.; Tsymbal, E. Y. Magnetic Nanoparticles: Recent Advances in Synthesis, Self-Assembly and Applications. *J. Mater. Chem.* **2011**, *21*, 16819–16845.

(3) Petit, C.; Taleb, A.; Pileni, M. P. Self-Organization of Magnetic Nanosized Cobalt Particles. *Adv. Mater.* **1998**, *10*, 259–261.

(4) Sun, S.; Murray, C. B. Synthesis of Monodisperse Cobalt Nanocrystals and Their Assembly into Magnetic Superlattices. *J. Appl. Phys.* **1999**, *85*, 8, 4325-4330.

(5) Puntes, V. F.; Krishnan, K. M.; Alivisatos, A .P. Colloïdal Nanocrystal Shape and Size control: The case of Cobalt. *Science*. **2001**, *291*, 2115-2117.

(6) Puntes, V. F.; Krishnan, K. M.; Alivisatos, A. P. Synthesis of Colloidal Cobalt Nanoparticles with Controlled Size and Shapes. *Topics in Catalysis*. **2002**, *19*, 145-147.

(7) Lisiecki, I.; Pileni, M. P. Synthesis of Well-Defined and Low Size Distribution Cobalt Nanocrystals: The Limited Influence of Reverse Micelles. *Langmuir*. **2003**, 16, 9486–9489.

(8) Soumare, Y.; Garcia, C.; Maurer, T.; Chaboussant, G.; Ott, F.; Fievet, F.; Piquemal, J. Y.; Viau, G. Kinetically Controlled Synthesis of Hexagonally Close-Packed Cobalt Nanorods with High Magnetic Coercivity. *Adv. Funct. Mater.* **2009**, *19*, 1971–1977.

(9) Puntes, V. F.; Zanchet, D.; Erdonmez, C. K.; Alivisatos, A. P. Synthesis of hcp-Co Nanodisks. *J. Am. Chem. Soc.* **2002**, *124*, 12874–12880.

(10) Dumestre, F.; Chaudret, B.; Amiens, C.; Fromen, M. C.; Casanove, M. J.; Renaud, P.; Zurcher, P. Shape Control of Thermodynamically Stable Cobalt

Nanorods through Organometallic Chemistry. *Angew. Chemie - Int. Ed.* **2002**, *41*, 4286–4289.

(11) Dinega, D. P.; Bawendi, M. G. A Solution-Phase Chemical Approach to a New Crystal Structure of Cobalt. *Angew. Chem*. **1999**, *38*, 1788-1791.

(12) Murray, C. B.; Sun, S.; Gaschler, W.; Doyle, H.; Betley, T. A.; Kagan, C. R. Colloidal Synthesis of Nanocrystals and Nanocrystal Superlattices. *IBM J. Res. Dev.* **2001**, *45*, 47–56.

(13) Parker, D.; Lisiecki, I.; Salzemann, C.; Pileni, M. P. Emergence of New Collective Properties of Cobalt Nanocrystals Ordered in Fcc Supracrystals: II, Magnetic Investigation. *J. Phys. Chem. C*. **2007**, *111*, 12632–12638.

(14) Polli, D.; Lisiecki, I.; Portalès, H.; Cerullo, G.; Pileni, M. P. Low Sensitivity of Acoustic Breathing Mode Frequency in Co Nanocrystals upon Change in Nanocrystallinity. *ACS Nano.* **2011**, *5*, 5785–5791.

(15) Yang, Z.; Lisiecki, I.; Walls, M.; Pileni, M. P. Nanocrystallinity and the Ordering of Nanoparticles in Two-Dimentional Superlattices: Controlled Formation of Either Core/Shell (Co/CoO) or Hollow CoO Nanocrystals. *ACS Nano.* **2013**, *7*, 1342-1350.

(16) Iablokov, V.; Beaumont, S. K.; Alayoglu, S.; Pushkarev, V. V.; Specht, C.; Gao, J.; Alivisatos, A. P., Kruse, N.; Somorjai, G. A. Size-Controlled Model Co Nanoparticle Catalysts for CO2 Hydrogenation: Synthesis, Characterization, and Catalytic Reactions. *Nano Letters* **2012**, *12*, 3091-3096.

(17) Shukla, N.; Svedberg, E. B.; Ell, J.; Roy, A. J. Surfactant Effects on the Shapes of Cobalt Nanoparticles. *Mater. Lett.* **2006**, *60*, 1950–1955.

(18) Wu, N.; Fu, L.; Su, M.; Aslam, M.; Wong, K. C.; Dravid, V. P. Interaction of Fatty Acid Monolayers with Cobalt Nanoparticles. *Nano Lett.* **2004**, *4*, 383–386.

(19) Petit, C.; Lixon, P.; Pileni, M. P. Structural Study of Divalent Metal bis(2-Ethylhexyl) Sulfosuccinate Aggregates. *Langmuir*. **1991**, *7*, 2620–2625.

(20) Eastoe, J.; Towey, T. F.; Robinson, B. H.; Williams, J.; Heenan, R. K. Structures of Metal bis(2-Ethylhexylsulfosuccinate) Aggregates in Cyclohexane. *J. Phys. Chem.* **1993**, *97*, 1459–1463.

(21) Gutierrez, J. A.; Falcone, R. D.; Lopez-Quintela, M. A.; Buceta, D.; Silber, J. J.; Correa, N. M. On the Investigation of the Droplet-Droplet Interactions of Sodium 1,4-bis(2-Ethylhexyl) Sulfosuccinate Reverse Micelles upon Changing the External Solvent Composition and Their Impact on Gold Nanoparticle Synthesis. *Eur. J. Inorg. Chem.* **2014**, 12, 2095–2102.

(22) Lisiecki, I.; Andre, P.; Filankembo, A.; Petit, C.; Tanori, J.; Gulik-Krzywicki, T.; Ninham, B. W.; Pileni, M. P. Mesostructured Fluids. 1. $Cu(AOT)_2$-H_2O-Isooctane in Oil Rich Regions. *J. Phys. Chem*. B. **1999**, *103*, 9168-9175.

(23) Lisiecki, I.; Andre, P.; Filankembo, A.; Petit, C.; Tanori, J.; Gulik-Krzywicki, T.; Ninham, B. W.; Pileni, M. P. Mesostructured Fluids. 2. *J. Phys. Chem*. B. **1999**, *103*, 9176-9189.

(24) Hansen C. M. Hansen's solubility parameters: A user's Handbook, CRC Press, Boca Raton **2000**.

(25) Barton F. M, Handbook of Solubility Parameters and others Cohesion Parameters, CRC Press, Boca Raton **1983**.

(26) Adhikari, N. P.; Peng, X.; Alizadeh, A.; Ganti, S.; Nayak, S. K.; Kumar, S. K. Multiscale Modeling of the Surfactant Mediated Synthesis and Supramolecular Assembly of Cobalt Nanodots. *Phys. Rev. Lett.* **2004**, *93*, 1–4.

(27) Khan, S. J.; Pierce, F.; Sorensen, C. M.; Chakrabarti, A. Self-Assembly of Ligated Gold Nanoparticles: Phenomenological Modeling and Computer Simulations. *Langmuir*. **2009**, *25*, 13861–13868.

(28) Goubet, N.; Richardi, J.; Albouy, P.A.; Pileni, M. P. How to Predict the Growth Mechanism of Supracrystals from Gold Nanocrystals. *J. Phys. Chem. Lett.* **2011**, *2*, 417–422.

(29) Lisiecki, I.; Pileni, M. P. Synthesis of Copper Metallic Clusters Using Reverse Micelles as Microreactors. *J. Am. Chem. Soc*. **1993**, *115*, 3887-3896.

(30) Petit, C.; Lixon, P.; Pileni, M. P. In-Situ Synthesis of Silver Nanocluster in Aot Reverse Micelles. *J. Phys. Chem.* **1993**, *97*, 12974–12983.

(31) Pileni, M. P.; Motte, L.; Petit, C. Synthesis of Cadmium Sulfide in Situ in Reverse Micelles: Influence of the Preparation Modes on Size, Polydispersity, and Photochemical Reactions. *Chem. Mater.* **1992**, *4*, 338–345.

(32) Murray, C. B.; Kagan, C. R.; Bawendi, M. G. Self-Organization of CdSe Nanocrystallites into Three-Dimensional Quantum Dot Superlattices. *Science.* **1995**, *270*, 1335–1338.

(33) Tovstun, S. A; Razumov, V. F. Preparation of Nanoparticles in Reverse Microemulsions. *Russ. Chem. Rev.* **2011**, *80*, 953–969.

(34) Lisiecki, I. Size, Shape, and Structural Control of Metallic Nanocrystals. *J. Phys. Chem. B*. **2005**, *109*, 12231–12244.

(35) Robertus, C.; Philipse, W. H.; Joosten, G. H.; Levine, Y. K. Solution of the Percus–Yevick Approximation of the Multicomponent Adhesive Spheres System Applied to the Small Angle X-Ray Scattering from Microemulsions. *J. Chem. Phys.* **1989**, *90*, 4482-4490.

(36) Towey, T. F.; Khan-Lodl, A.; Robinson, B. H. Kinetic and Mechanism formation of Quantum-sized Cadmium Sulfide in Water Aerosol-OT Microemulsions. *J. Chem. Soc., Faraday Trans.* **1990**, *2*, 86, 3757-3762.

(37) Pitre, F.; Regnaut, C.; Pileni, M. P. Structural Study of AOT Reverse Micelles Containing Native and Modified alpha-Chymotrypsin. *Langmuir*. **1993**, *9*, 2855–2860.

(38) Gutierrez, J. A; Alejandra Luna, M.; Mariano Correa, N; Silber, J. J; Dario Falcone, R. The impact of the polar core size and external organic media

composition on micelle-micelle interactions: the effect on gold nanoparticle synthesis. *New J. Chem*. **2015**, 39, 8887-8895.

(39) Lisiecki.I. Oral Communication: Self-organization and Nanocrystallinity Effects of 7 nm-Co Nanoparticles on the Magnetic, Vibration Properties and Oxidation Process. *T MP0904 Action, Single and multiphase ferroics and multiferroics with restricted geometries, Closing Conference and Final MC meeting.* Genoa, Italy, **2014**.

(40) Zeng, Q.; Jiang, X.; Yu, A.; Lu, G. M. Growth Mechanisms of Silver Nanoparticles: A Molecular Dynamics Study. *Nanotechnology.* **2007**, *18*, 35708-35715.

(41) Lisiecki, I.; Pileni, M. P. Long-Range 2D and 3D Self-Organizations of Co Nanocrystals: A New Challenge for a New Physics. *Comptes Rendus Chim.* **2009**, *12*, 235–246.

(42) Parker, D.; Lisiecki, I.; Pileni, M. P. Do 8 Nm Co Nanocrystals in Long-Range-Ordered Face-Centered Cubic (Fcc) Supracrystals Show Superspin Glass Behavior? *J. Phys. Chem. Lett.* **2010**, *1*, 1139–1142.

(43) Lisiecki, I.; Polli, D.; Yan, C.; Soavi, G.; Duval, E.; Cerullo, G.; Pileni, M. P. Coherent Longitudinal Acoustic Phonons in Three-Dimensional Supracrystals of Cobalt Nanocrystals. *Nano Lett.* **2013**, *13*, 4914–4919.

(44) Lisiecki, I.; Albouy, P.A.; Pileni, M. P. Face-Centered-Cubic “Supracrystals” of Cobalt Nanocrystals. *Adv. Mater.* **2003**, *15*, 712–716.

(45) Del Fatti, N.; Voisin, C.; Chevy, F.; Vallée, F.; Flytzanis, C. Coherent Acoustic Mode Oscillation and Damping in Silver Nanoparticles. *J. Chem. Phys.* **1999**, *110*, 11484.

(46) Duval, E. Far-Infrared and Raman Vibrational Transitions of a Solid Sphere: Selection Rules. *Phys. Rev. B.* **1992**, *46*, 5795–5797.

(47) Gouadec, G.; Colomban, Ph. Raman Spectroscopy of Nanomaterials: How Spectra Relate to Disorder, Particle Size and Mechanical Properties. *Prog. Cryst. Growth Charact. Mater.* **2007**, *53*, 1–56.

(48) Duval, E.; Saviot, L.; Mermet, A.; Murray, D. B. Continuum Elastic Sphere Vibrations as a Model for Low Lying Optical Modes in Icosahedral Quasicrystals. *J. Phys. Condens. Matter* **2005**, *17*, 3559-3565.

(49) Simon, G.; Meziane, L.; Courty, A.; Colomban, Ph.; Lisiecki, I. Low Wavenumber Raman Scattering of Cobalt Nanoparticles Self-Organized in 3D Superlattices far from Surface Plasmon Resonance. *J. Raman Spectrosc*. **2016**, *2*, 248-251.

(50) Hernandez-Rosas, J.; Picquart, M.; Haro-Poniatowski, E.; Kanehisa, M.; Jouanne, M.; Morhange, J. F. Elastic Vibrations of Spheroidal Nanometric Particles. *J. Physics-Condensed Matter*. **2003**, *15*, 7481–7487.

(51) Zhang, P.; Sui, Y.; Xiao, G.; Wang, Y.; Wang, C.; Liu, B.; Zou, G.; Zou, B. Facile fabrication of faceted copper nanocrystals with high catalytic activity for p-nitrophenol reduction. *J. Mater. Chem. A*. **2013**, 5, 1632-1638.

(52) Zhang, P.; Sui, Y.; Wang, C.; Wang, Y.; Cui, G.; Wank Ch.; Liu. B.; Zou, B. A one-step green route to synthesize copper nanocrystals and their applications in catalysis and surface enhanced Raman scattering. *Nanoscale*. **2014**, 6, 5343-5350.

(53) Wang C.; Xiao G.; Sui Y.; Yang X.; Liu G.; Jia M.; Han W.; Liu B.; Zou B. Synthesis of dendritic iridium nanostructures based on the oriented attachment mechanism and their enhanced CO and ammonia catalytic activities. *Nanoscale*. **2014**, 6, 15059-15065.

(54) Wang, C.; Sui, Y.; Xiao, Y.; Wei, Y.; Zou, G.; Zou, B. Synthesis of Cu-Ir nanocages enhanced electrocatalytic activiy for the oxygen evolution reaction. *J. Mater. Chem. A*. **2015**, 3, 19669-19673.

(55) Man, X.; Sui, Y.; Zang, C.; Zhou, B.; Wei, Y.; Zou, B. Design of porous Ag platelet structures with tunable porosity and high catalytic activity. *J. Mater. Chem. A*. **2015**, 3, 22339-22346.

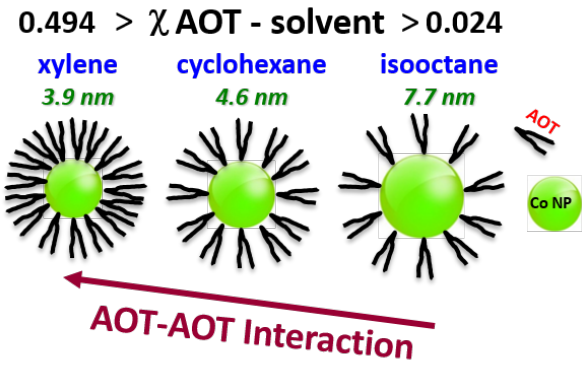
0.494 > χ AOT - solvent > 0.024
xylene
cyclohexane
isooctane
3.9 nm
4.6 nm
7.7 nm
AOT
Co NP
AOT-AOT Interaction